



Stable tissue-simulating phantoms with various water and lipid contents for diffuse optical spectroscopy

ETSUKO OHMAE,^{1,*} NOBUKO YOSHIZAWA,² KENJI YOSHIMOTO,¹ MAHO HAYASHI,² HIROKO WADA,¹ TETSUYA MIMURA,¹ HIROAKI SUZUKI,¹ SHU HOMMA,¹ NORIHIRO SUZUKI,¹ HIROYUKI OGURA,³ HATSUKO NASU,² HARUMI SAKAHARA,² YUTAKA YAMASHITA,¹ AND YUKIO UEDA¹

¹Central Research Laboratory, Hamamatsu Photonics K. K., 5000, Hirakuchi, Hamakita-ku, Hamamatsu City, Shizuoka Pref., 434-8601, Japan

²Department of Diagnostic Radiology and Nuclear Medicine, Hamamatsu University School of Medicine, 1-20-1 Handayama, Higashi-ku, Hamamatsu City, Shizuoka Pref., 431-3192, Japan

³Department of Breast Surgery, Hamamatsu University School of Medicine, 1-20-1 Handayama, Higashi-ku, Hamamatsu City, Shizuoka Pref., 431-3192, Japan

*etuko-o@crl.hpk.co.jp

Abstract: We introduced a method for producing solid phantoms with various water-to-lipid ratios that can simulate the absorption, and to some extent the scattering characteristics of human breast tissue. We also achieved phantom stability for a minimum of one month by solidifying the emulsion phantoms. The characteristics of the phantoms were evaluated using the six-wavelength time-domain diffuse optical spectroscopy (TD-DOS) system we developed to measure water and lipid contents and hemoglobin concentration. The TD-DOS measurements were validated with a magnetic resonance imaging system.

© 2018 Optical Society of America under the terms of the [OSA Open Access Publishing Agreement](#)

1. Introduction

Near-infrared spectroscopy (NIRS) in the range of 650–1000 nm is used widely to non-invasively acquire light absorption information of hemoglobin, water, and lipids in various human tissues. Water and lipid contents are necessary to measure the properties of breast tissue [1–8]. Several studies have evaluated the use of NIRS to monitor tumor response to neoadjuvant chemotherapy (NAC) for breast cancer. In this application, it is important to measure water and lipid content and hemoglobin concentration accurately. These parameters depend on the presence or absence of tumors [9] and breast density [10], and reflect angiogenic activity, inflammatory response, and edema volume. Therefore, they may become a prognostic biomarker in NAC [11–13].

Tissue simulating phantoms such as Intralipid-based aqueous phantoms [14,15] and resin-based hard phantoms are commonly used to evaluate the performance of NIRS systems [16]. A phantom with water and lipid content that can be controlled is also necessary to assess the ability of a NIRS system to measure these contents. Previous studies have proposed phantoms with various water and lipid contents [17–20]. Merritt et al. [17] reported on an emulsion phantom made using Triton X-100 as the emulsifier. The results showed good correlation between diffuse optical spectroscopic imaging (DOSI) and magnetic resonance imaging (MRI). The reduced scattering coefficients of their phantoms were not mentioned in Merritt et al. [17]; however, Quarto et al. [18] constructed a phantom following the same procedures and reported reduced scattering coefficients. The reduced scattering coefficients of human breast tissue, measured with the subject in a supine position, range from about 5–15 cm⁻¹ [21]. The reduced scattering coefficient of the phantom that Quarto et al. [18] reported had higher values than that of the human breast tissue it was compared to. Nachabé [19] analyzed water

and lipid contents at longer wavelengths (900–1600 nm) by using diffuse optical spectroscopy (DOS) and also found a reduced scattering coefficient higher than the reported value. The emulsifier Triton X-100 was used in all these studies; however, it has been designated a hazardous substance by the Globally Harmonized System (GHS) of Classification and Labelling of Chemicals. Michaelsen et al. [20] used guar gum to mix water and lard without any emulsifier and the scattering properties of the phantom were close to human breast tissue. They also created anthropomorphic phantoms mimicking the complex tissue geometry of a breast with a tumor. However, their phantoms were tested for durability for only two weeks. The phantoms with high lipid ratios required remixing after solidification to achieve homogeneity; thicker and larger phantoms also had to be remixed for the same reason.

In this study, we constructed water/lipid phantoms with reduced scattering coefficients in the range reported for human breast tissue, created with harmless substances, and hardly demulsified. The measurement results of an MRI, defined as a “gold standard” technique by Merritt et al. [17], were employed to evaluate the phantoms. MR images enable us to confirm the internal uniformity of the constructed phantoms while measuring water and lipid content. In this paper, we present the MRI results that confirm that our phantoms were created with the desired ratios and present the results of measuring the same phantoms using our six-wavelength time-domain diffuse optical spectroscopy (TD-DOS) system. We also investigated the long-term stability of the phantoms using our TD-DOS system.

2. Materials and methods

2.1 Six-wavelength time-domain diffuse optical spectroscopy (TD-DOS) system

2.1.1 Instrumentation

The six-wavelength TD-DOS system (TRS-21-6W) was constructed based on a three-wavelength system we had previously developed (TRS-20, Hamamatsu Photonics K.K.) to measure hemoglobin concentrations in human muscle, brain, and breast tissue [21–25]. That system, the TRS-20, is a dual-channel TD-DOS system that uses three wavelengths in the 750 nm to 850 nm range. The TRS-21-6W was built by replacing one of the two channels of TRS-20 with a light source and photodetector unit designed to measure three wavelengths in the 900 nm to 1000 nm range. This was done to enable measurement of six wavelengths in the 750 nm to 1000 nm range and quantify hemoglobin concentration, and water and lipid content.

The TRS-21-6W consists of two light source units, two photodetector units, a single photon counting (SPC) circuit, and optical fiber bundles (Fig. 1). The light source units (custom-designed, Hamamatsu Photonics K.K.) are composed of three laser diodes per unit (762 nm, 802 nm, and 838 nm for unit 1; 908 nm, 936 nm, and 976 nm for unit 2). Each laser diode emits a pulse 100 ps to 200 ps wide (full width at half maximum) at a repetition rate of 5 MHz. A specimen was irradiated with the pulsed laser through a source optical fiber bundle 1 mm in diameter with a numerical aperture (NA) of 0.29 (Sumita Optical Glass, Inc). The light that propagated through the specimen was collected by a detection fiber bundle 3 mm in diameter and with an NA of 0.29 (Sumita Optical Glass, Inc) and guided to two photodetector units containing different photomultiplier tubes (GaAs and InGaAs PMT, Hamamatsu Photonics K.K.). A variable optical attenuator (VOA; custom-designed, Hamamatsu Photonics K.K.) with an attenuation range of 0 dB to 45 dB was used to reduce the power level of the detected light. The VOA designed for the TRS-21-6W has 81 attenuation steps; this enables the system to carry out a measurement at a more appropriate attenuation level compared to the 9-step VOA used in the TRS-20. The detected light was converted into an electrical signal by the photodetector units and processed with a custom-designed SPC circuit consisting of a constant fraction discriminator (CFD), time-to-amplitude converter (TAC), an analog-to-digital (A/D) converter, and a histogram memory. The processed signal was acquired as a temporal profile of the detected light. To measure the optical properties more

accurately by reducing the influence of the NA of the detection fiber bundle, we placed a thin diffuser slab in front of the detection optical fiber during the instrument response function (IRF) measurements [26]. Figure 2 shows the IRF at all wavelengths. The specifications of the TRS-21-6W are listed in Table 1.

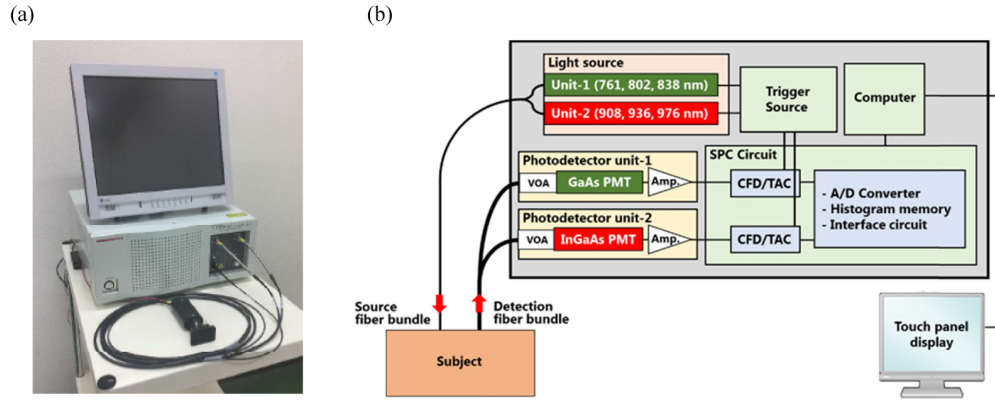


Fig. 1. TRS-21-6W: (a) appearance and (b) block diagram.

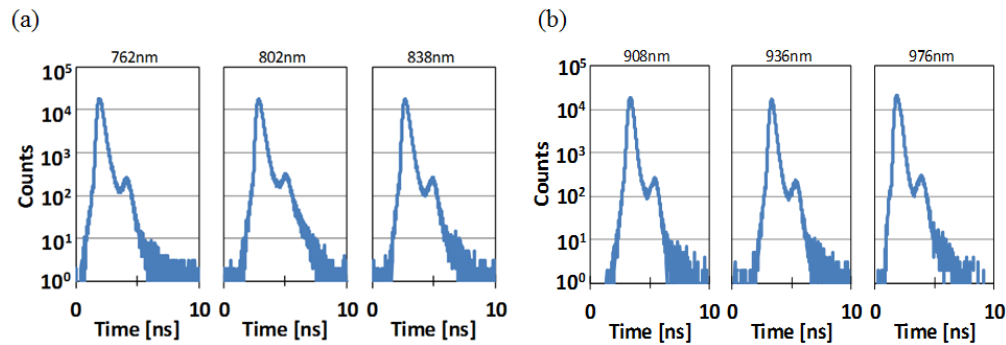


Fig. 2. IRF at all wavelengths: (a) unit 1 and (b) unit 2.

Table 1. Specifications of TRS-21-6W.

Component	Features	Unit 1	Unit 2
Light source	Wavelengths	762, 802, 838 [nm]	908, 936, 976 [nm]
	Spectral width at each wavelength (FWHM)	< 3[nm]	< 4 [nm]
	Pulse width at each wavelength (FWHM)	< 100 ps	< 200 [ps]
	Output power at optical fiber end for each wavelength	< 100 [μ W]	< 400 [μ W]
	Pulse repetition rate	5 [MHz]	
PMT	Photocathode	GaAs	InGaAs
	Quantum efficiency	12%(at 800nm)	1% (at 900nm)
	Transit time spread (FWHM)	< 400 [ps]	
SPC Circuit	Dead time	400 [ns]	
	A/D Converter	13 [bit] (SAR ADC)	
	Histogram memory	16 [bit] x 8192 x 2	
	Differential Non-Linearity (DNL)	< 0.015 [LSB] (typical)	
	Integral Non-Linearity (INL)	< 0.15 [LSB] (typical)	
Others	Time bin width	10 [ps]	
	Dimensions	430(W) x 465(D) x 170(H)mm	

2.1.2 Measurement

We measured a liquid phantom to evaluate the basic performance of the system and water/lipid solid phantoms to check their optical properties and long-term stability. The TD-DOS system is able to quantify the optical properties of a specimen by analyzing the temporal profiles measured in reflectance and transmittance geometry. In this study, the reflectance geometry measurements were carried out with a source-detector separation of 20 mm and an acquisition time of 5 s to 8 s.

2.1.3 Data analysis

The TD-DOS system provides absorption (μ_a) and reduced scattering (μ'_s) coefficients in a scattering medium such as biological tissue by analyzing the measured temporal profiles based on photon diffusion theory. The behavior of photons in a homogeneous scattering medium is expressed by the photon diffusion equation [27]:

$$\frac{1}{c} \frac{\partial}{\partial t} \phi(\mathbf{r}, t) - D \nabla^2 \phi(\mathbf{r}, t) + \mu_a \phi(\mathbf{r}, t) = S(\mathbf{r}, t), \quad (1)$$

where $\phi(\mathbf{r}, t)$ is the diffuse photon fluence rate at position \mathbf{r} and time t , $D = 1/(3(\mu_a + \mu'_s))$ is the photon diffusion coefficient, c is the speed of light in the medium, and $S(\mathbf{r}, t)$ is a source term.

The TD-DOS system uses the analytical solutions of the photon diffusion equation obtained with several types of boundary conditions to analyze the temporal profiles measured in reflectance and transmittance geometries. In this subsection, we mention only the diffuse reflectance because all phantoms were measured in reflectance geometry. The diffuse reflectance $R(d, t)$ derived from the solution of Eq. (1) for a semi-infinite homogeneous model with extrapolated boundary condition is expressed as follows:

$$R(d, t) = \frac{1}{2} (4\pi Dc)^{-3/2} t^{-5/2} \exp(-\mu_a ct) \cdot \left[z_0 \exp\left(-\frac{z_0^2 + d^2}{4Dct}\right) + (z_0 + 2z_e) \exp\left(-\frac{(z_0 + 2z_e)^2 + d^2}{4Dct}\right) \right], \quad (2)$$

where d is the source-detector separation on the planar surface, $z_0 = 1/(\mu_a + \mu'_s)$ is the transport mean free path and $z_e = 2D(1+r_d)/(1-r_d)$ is the linear extrapolation distance [28]. r_d is the internal reflectance due to a refractive index mismatch at the boundary, which is calculated from an approximate expression ($r_d = -1.440n^{-2} + 0.710n^{-1} + 0.668 + 0.0636n$) that depends on the refractive index of the medium ($n = n_{\text{tissue}}/n_{\text{air}}$) [28]. Based on Eq. (2), an estimated temporal profile was obtained by calculating the convolution of the IRF with $R(d, t)$ for each considered (μ_a, μ'_s) pair to take into account the effect of the IRF [29, 30]. μ_a and μ'_s of the medium were then determined by fitting the estimated profile to the measured profile with a non-linear least squares method based on the Levenberg-Marquardt algorithm.

The absorption coefficient obtained for each wavelength λ is expressed with the following linear combination:

$$\mu_a(\lambda) = \sum_{i=1}^m C_i \varepsilon_i(\lambda), \quad (3)$$

where m is the number of considered tissue chromophores, C_i is the concentration, and $\varepsilon_i(\lambda)$ is the extinction coefficient of the i -th chromophore. If the extinction coefficients of all contributing chromophores can be measured with a spectrophotometer, their

concentrations can be determined by solving the system of linear equations of Eq. (3). The major chromophores in biological tissue at near-infrared wavelengths are deoxy-hemoglobin, oxy-hemoglobin, water, and lipid. The purpose of this study is to establish the preparation procedures of the water/lipid phantoms and to evaluate their characteristics. In order to achieve our aim, any absorption agent (e.g. ink, blood, etc.) was not added to the phantoms. Therefore, the investigated phantoms contained only water and lipid, as well as emulsifier and solidifying agent. The absorption spectrum of lecithin used as emulsifier (see Section 2.3) was measured with a spectrophotometer (U-3500, Hitachi High-Technologies Corporation, Tokyo, Japan) and its absorption coefficient was very small in the wavelength range of 700–1000 nm. In addition, the proportion of coagulant in the phantom was very low. For the reason above, we assumed that the absorption of the emulsifier and solidifying agent is negligible, so that only water and lipid need to be considered in the data analysis. The water absorption spectrum was also measured with the spectrophotometer. The lipid absorption spectrum that we used was reported in the literature [31]. The absorption spectra of water and lipid are shown in Fig. 3.

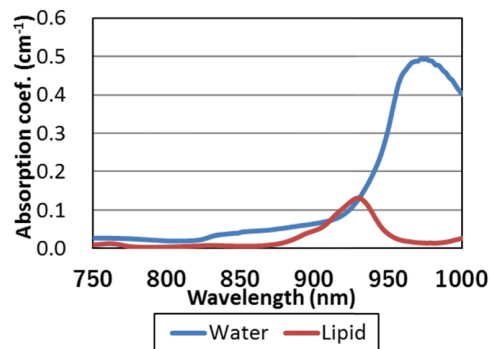


Fig. 3. Absorption spectra of water and lipid.

2.1.4 Evaluating the performance of the six-wavelength TD-DOS system

The basic performance of the TD-DOS system was evaluated by measuring a liquid phantom series made from a mixture of lipid emulsion (50 mL Intralipos Injection 20%; Otsuka Pharmaceutical Co., Ltd.), heavy water (950 mL D₂O; Merck Millipore Chemicals), and different amounts of carbon ink (Kiwa-Guro, Sailor Pen Co., Ltd.). The amount of carbon ink in the basic 1% Intralipos phantom emulsion was gradually increased from 0 mL in 0.2 mL (0.02%) steps to confirm the accuracy of μ_a and the dynamic range of the TD-DOS system. To prepare the basic phantom emulsion, D₂O was used instead of H₂O, because it provided a very low base value of μ_a in the near-infrared region (650–1000 nm) [33]. Therefore, by varying the amount of carbon ink in the phantom, the μ_a values of the liquid phantom series could be adjusted over the relevant dynamic range (0 to 0.3 cm⁻¹ for human breast tissue in the near-infrared range [1,32]). Due to the high absorption coefficient of H₂O in the near-infrared range, this would not have been possible when using H₂O instead of D₂O to prepare the basic phantom emulsion. For example, the μ_a value of pure H₂O without carbon ink is already 0.5 cm⁻¹ at 976 nm, the peak position in its absorption spectrum (see Fig. 3).

2.2 MRI

Data acquisition was performed with a 3.0T MR unit (Discovery 750w, GE Healthcare, Waukesha, WI). The proton density fat fraction (PDFF) [34,35] pulse sequence used for this study was the commercially available sequence provided by the manufacturer of the MR unit

(IDEAL IQ, GE Healthcare). The pulse sequence is the multipoint Dixon technique that uses a low flip angle to limit T1 bias, acquires six echoes to correct for T2* effects, and uses a multipeak fat model. The parameters of this sequence were as follows: repetition time, 7.3 ms; shortest echo time, 3 ms; field of view, 40×40 cm; matrix, 160×160 ; bandwidth, 111.1 kHz; flip angle, 4° ; section thickness, 7 mm; and a single dimensional image with 36 sections. The images were processed using the software provided by the manufacturer (IDEAL IQ, GE Healthcare) to instantaneously create water, fat, R2*, and fat fraction maps. The data were acquired twice and two additional measurements were performed after rearranging the phantoms in the reverse direction. The fat fraction of the phantoms was measured with a medical imaging system (SYNAPSE version 4.1, Fujifilm Medical, Tokyo, Japan). The water fraction was quantified by subtracting the fat fraction from 100%.

2.3 Procedure to make the water/lipid phantom

The solid tissue phantoms were solidified emulsions containing distilled water and either a combination of soybean oil (Riken Nosan-Kako Co. Ltd.) and soybean lecithin (FUJIFILM Wako Pure Chemical Corporation) or (in one case) Intralipos containing, among others, soybean oil and egg lecithin. A coagulant (agar or an oil-solidifying agent) was added for solidification to achieve long-term stability. The employed oil-solidifying agent is made from castor oil, available in powder form at room temperature, and commonly used to solidify cooking oil for easier disposal in Japan. We devised three procedures to make a solid phantom with various water-to-lipid ratios and reduced scattering coefficients in the range of human breast tissue. A set of six phantoms was made for the evaluation with water-to-lipid ratios (by volume) of 99:1, 80:20, 60:40, 40:60, 20:80, and 5:95.

The three emulsions with water-to-lipid ratios of 99:1, 80:20 and 60:40 were prepared as oil-in-water (O/W) emulsions and solidified with agar. The three emulsions with water-to-lipid ratios of 40:60, 20:80 and 5:95 were prepared as water-in-oil (W/O) emulsions and solidified with oil-solidifying agent. The container size was $151 \text{ mm} \times 151 \text{ mm} \times 90 \text{ mm}$, and the amount of emulsion was 1 L for each phantom.

The water and lipid contents of each phantom were measured with the six-wavelength TD-DOS system and MRI to compare the results to the theoretical values. A TD-DOS system probe was positioned at the center of the planar phantom surface. For the fat fraction maps obtained by MRI, a $2 \text{ cm} \times 5 \text{ cm}$ rectangular region of interest (ROI) was placed just below the surface at the horizontal center of the phantoms. A mean value of four measurements was obtained for each phantom.

2.3.1 Water/lipid phantom with a water-to-lipid ratio of 99:1

The water was heated to boiling and agar equal to 5% of the water mass was added. After the agar dissolved completely, the mixture was filtered through a fine-mesh net to remove agar fragments and was allowed to cool to 60°C . In a separate container, the agar mixture (950 mL) and Intralipos 20% (50 mL) were mixed to create 1 L of emulsion of 1% Intralipos. The emulsion was poured into the container, which was then placed in an ice water bath, and stirred slowly with a glass rod. The container was stored in a refrigerator until the emulsion had set.

2.3.2 Water/lipid phantoms with water-to-lipid ratios of 80:20 and 60:40

In a container, lecithin (1 wt% of soybean oil) was added to soybean oil and heated at 60°C in a constant temperature water bath. In a separate container, water was heated to boiling and agar equal to 5% of the water mass was added. After the agar dissolved completely, the agar mixture was filtered through a fine-mesh net to remove agar fragments and was allowed to cool to 60°C .

For the water-to-lipid ratio of 80:20, the oil mixture (200 mL) was added to the agar mixture (800 mL) and blended together by a handheld blender until emulsified. For the water-

to-lipid ratio of 60:40, the oil mixture (400 mL) was added to 50% of the total water mass (300 mL) and blended together by a handheld blender until emulsified. Subsequently, the agar mixture (300 mL) was gradually added to the emulsion while stirring continuously with a glass rod. The emulsion was poured into the container, which was then placed in an ice water bath, and stirred slowly with a glass rod. The container was stored in a refrigerator until the emulsion had set.

2.3.3 Water/lipid phantoms with water-to-lipid ratios of 40:60, 20:80 and 5:95

Lecithin (1 wt% of soybean oil) and finely crushed oil-solidifying agent (15 g, 22.5 g, or 30 g depending on the water-to-lipid ratio) were added to soybean oil (550 mL, 800 mL, or 950 mL) in a container. The water was gradually added to the oil mixture up to the desired water-to-lipid ratio while mixing by a handheld blender. The resulting mixture was heated to 85°C in a constant temperature water bath while stirring continuously with a glass rod. After the oil-solidifying agent dissolved, the mixture was filtered through a fine-mesh net to remove oil-solidifying agent fragments. The emulsion was poured into the container, which was then placed in an ice water bath, and stirred slowly with a glass rod. The container was stored in a refrigerator until the emulsion had set. In addition to the water-in-oil (W/O) preparation procedure described here, an alternative oil-in-water (O/W) preparation procedure was investigated in case of the 40:60 emulsion. Results are discussed in Section 5.

3. Results

3.1 Evaluation of the performance of the six-wavelength TD-DOS system using a liquid phantom series

Figure 4 shows μ_a and μ'_s of the liquid phantoms obtained at each wavelength using the TD-DOS system. μ_a , which is a key factor to measure the accuracy of water and lipid content, showed a good linearity and, in particular for wavelength up to 838 nm, also a good absolute consistency with the theoretical value (Fig. 4 (a)). A small increase in μ'_s was observed as the amount of carbon ink increased (Fig. 4 (b)). The absolute μ'_s values vary between 8 and 12 cm^{-1} , which lies within the variation range 5 to 15 cm^{-1} reported for human breast tissue [21]. These results indicate that the six-wavelength TD-DOS system provides a sufficient dynamic range for investigations of human breast tissue whose absorption coefficient ranges from 0 to 0.3 cm^{-1} in the near-infrared region [1, 32].

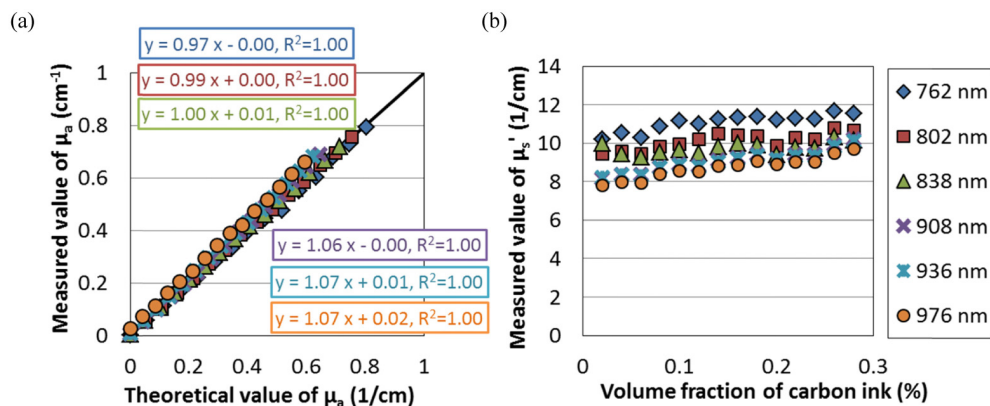


Fig. 4. (a) Absorption and (b) reduced scattering coefficients obtained from the liquid phantoms.

3.2 Evaluation of the solid tissue phantoms

The characteristics of six solid phantoms with water-to-lipid ratios of 99:1, 80:20, 60:40, 40:60, 20:80, and 5:95 are shown in Fig. 5. All phantoms were solidified with coagulants (see Section 2.3) and could be cut out easily without losing their shape. Photographs of the cut sections show that the phantoms are homogeneous. The lipid content (volume fraction) of each phantom was measured using MRI for different depths underneath the planar phantom surface. ImageJ/Fiji software was used to determine an average value within a 1 cm wide ROI in the center of the respective cross-sectional area for each depth value [36]. The depth dependence of the lipid content shown in Fig. 6 demonstrates the homogeneity of the phantom.


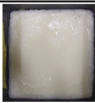












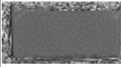
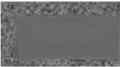


Water/Lipid		99:1	80:20	60:40	40:60	20:80	5:95
Type of emulsion		Oil-in-water (O/W)			Water-in-oil (W/O)		
Ingredients	Water	Distilled water					
	Lipid	Soybean oil (200 g/l in Intralipos® 20%)	Soybean oil				
	Emulsifier	Egg lecithin (12 g/l in Intralipos® 20%)	Soybean lecithin (1wt% of soybean oil)				
	Coagulant	Agar			Oil solidifying agent		
Photographs	Top down view						
	Cut section						
	MRI						

Fig. 5. Characteristics of the solid tissue phantoms.

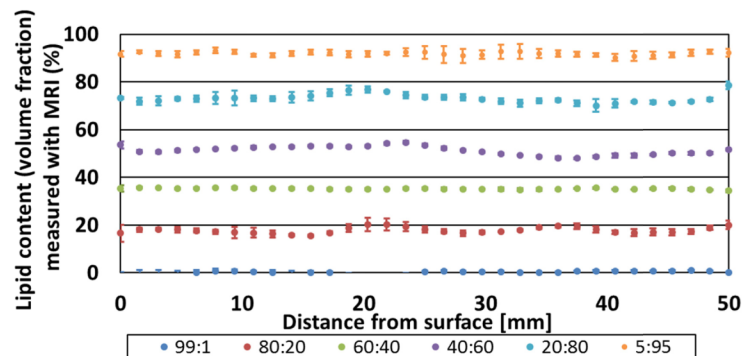


Fig. 6. Lipid content (volume fraction) in the solid tissue phantoms as obtained from MRI data for different depths underneath the planar phantom surface. At each depth, only a 1 cm wide ROI in the center of the respective cross-sectional area was analyzed.

Figure 7 shows the μ_a and μ'_s measured at each wavelength for the six phantoms. The μ'_s values fell in the range from 5 to 15 cm^{-1} , which is the range reported for human breast tissue [21]. Since all phantoms were made from water and lipids and no other chromophores were added, the μ_a values at 762 nm, 802 nm, and 836 nm were quite low compared to the value at the other three wavelengths, and the absolute changes in μ_a depending on the water-to-lipid ratio were small at wavelengths from 762 nm to 908 nm. The influence of the relative amount of water in the phantom can best be seen in the change in absorption at 976 nm. A slight influence can also be discerned at 936 nm.

Figure 8 shows the water and lipid contents of the phantoms measured with the six-wavelength TD-DOS system and MRI. The water and lipid volume fractions measured with MRI were close to the expected values (based on the water-to-lipid mixing ratio used for phantom preparation), which demonstrated that the phantoms could be successfully manufactured with the desired water-to-lipid ratios. Although the results measured with the TD-DOS system correlated well with the expected values, the slope and intercept of the regression line were 0.89 and -0.99% for water and 0.84 and 8.39% for lipids, respectively.

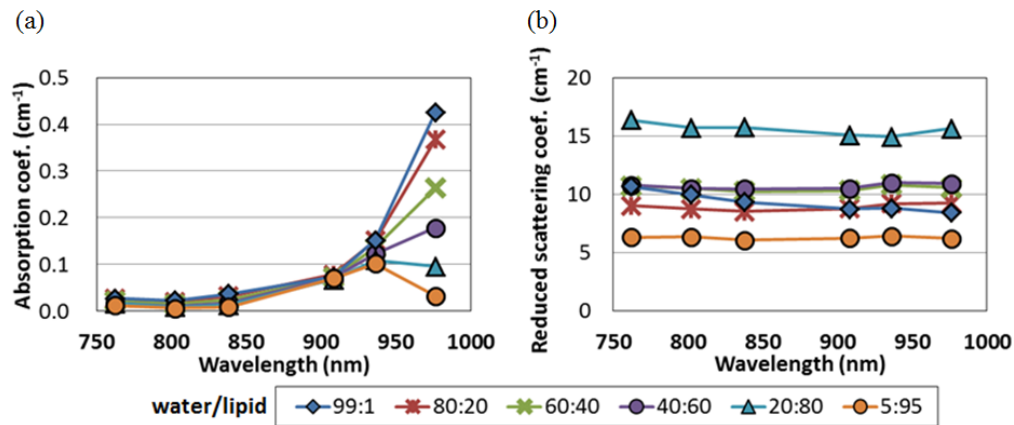


Fig. 7. (a) Absorption and (b) reduced scattering coefficients obtained by measuring six solid tissue phantoms using the six-wavelength TD-DOS system.

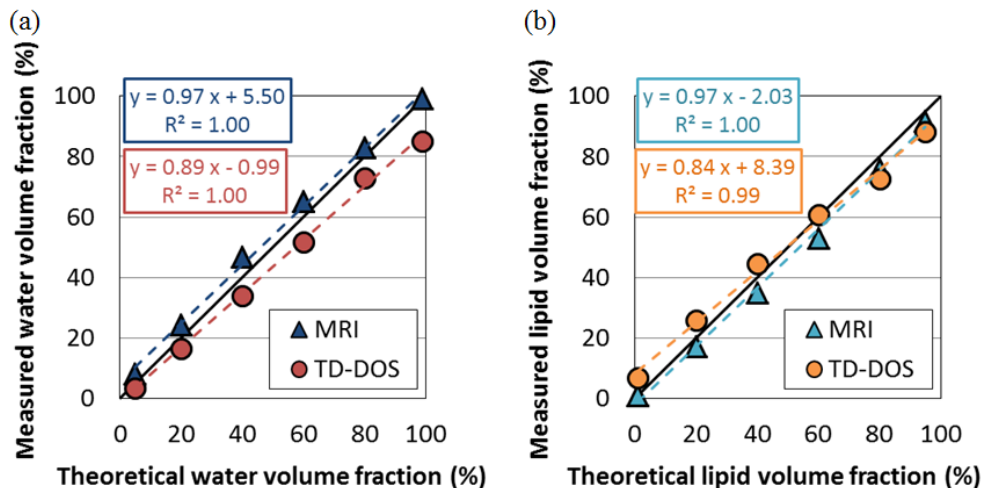


Fig. 8. (a) Water and (b) lipid volume fractions measured with TD-DOS system and MRI on solid tissue phantoms as a function of the corresponding theoretical volume fractions based on the phantom preparation procedure.

The measurements were carried out once a week for a period of two months to confirm the long-term stability of the phantoms. Figure 9 shows the stability of the optical properties and the water and lipid contents for the phantoms with water-to-lipid ratios of 80:20 and 40:60. The μ_a and the water and lipid content remained almost constant during this period. The μ'_s of the phantoms changed with time, depending on the water-to-lipid ratio; μ'_s of the phantoms with a higher percentage of water (water-to-lipid ratio of 99:1, 80:20, and 60:40) increased moderately, whereas that of the phantoms with a higher percentage of lipids (water-to-lipid ratio of 40:60 and 20:80) started to decrease strongly in a time-proportionally manner after one month. For the 5:95 phantom, μ'_s of the phantom was stable for two months, but oil separation was visually observed after one month. For all phantoms, the maximum changes in μ_a , μ'_s , and water and lipid content within one month after preparation were 0.022 cm^{-1} , 2.1 cm^{-1} , 5.9%, and 6.3%, respectively.

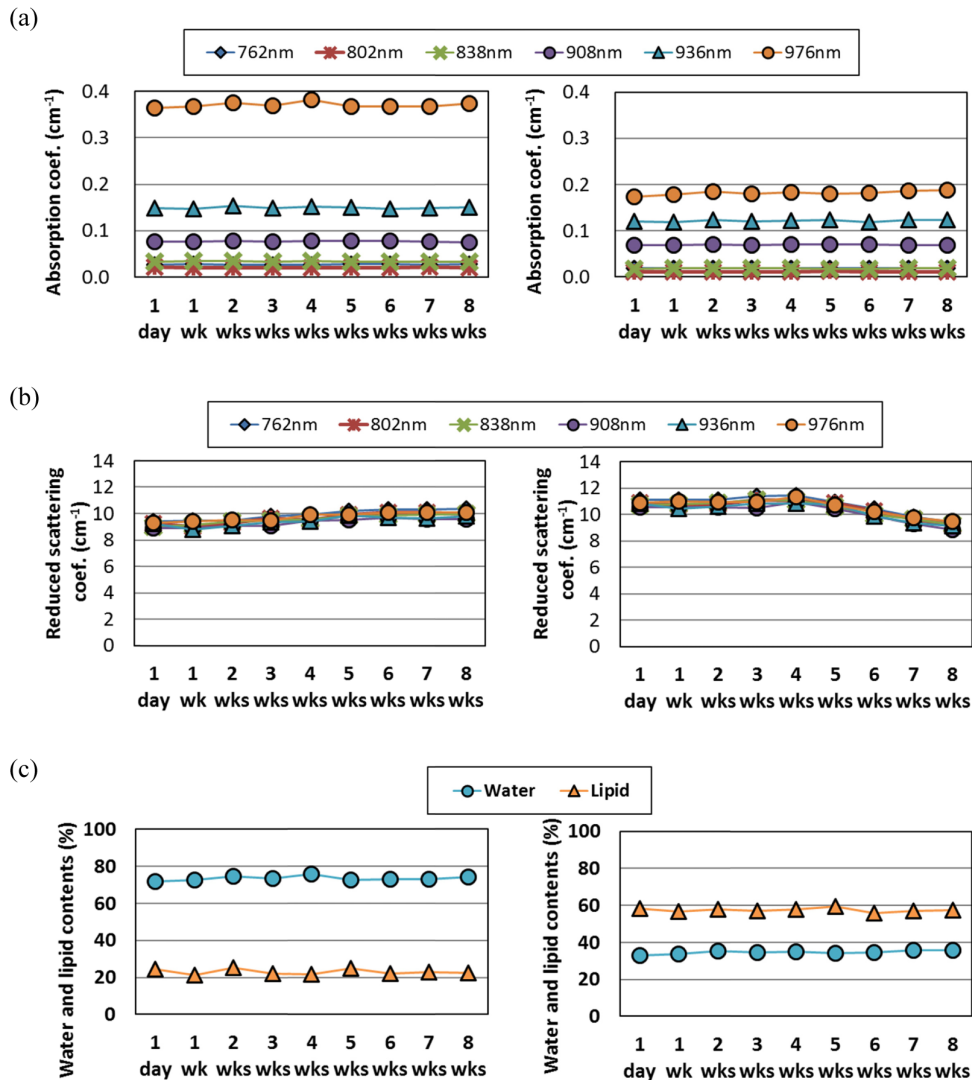


Fig. 9. Long-term stability of (a) absorption coefficient, (b) reduced scattering coefficient, and (c) water and lipid contents of the solid tissue phantoms with water-to-lipid ratios of 80:20 (left) and 40:60 (right). All measurement series started 1 day after phantom preparation.

4. Discussion

4.1 Evaluation of the performance of the six-wavelength TD-DOS system using a liquid phantom series

The six-wavelength TD-DOS system was developed with the perspective to quantitatively measure water and lipid contents and hemoglobin concentrations in biological tissue. The basic performance of the TD-DOS system was experimentally evaluated using a liquid phantom made with D₂O, lipid emulsion, and different amounts of carbon ink. By using D₂O instead of H₂O, we were able to examine the accuracy of the system in the low absorption region even at the wavelength 976 nm where H₂O exhibits a strong absorption maximum. The results showed a good correlation of the experimentally obtained μ_a values with the theoretical value and demonstrated that the TD-DOS system provides a wide dynamic range and high measurement accuracy.

4.2 Preparation of the water/lipid phantoms

To further verify the TD-DOS system, we established a method to create solid phantoms with various water-to-lipid ratios and scattering characteristics in the range of human breast tissue. We devised three procedures to make a phantom, which differ depending on the phantom water-to-lipid ratio. Procedures were developed for a phantom with a water-to-lipid ratio of 99:1, for phantoms with water-to-lipid ratios of 80:20 and 60:40, and for phantoms with water-to-lipid ratios of 40:60, 20:80, and 5:95.

4.2.1 Comparison of different liquid emulsion preparation procedures for 40:60 emulsions

As a preparatory step, liquid emulsions with a water-to-lipid ratio of 40:60 (similar to human breast tissue) were prepared with two different preparation procedures and compared. Oil and water are normally immiscible, but an emulsion can be achieved with proper mixing and the aid of emulsifiers (soybean lecithin in this part of the study). In general, there are two types of emulsions: oil-in-water (O/W) and water-in-oil (W/O). The O/W emulsion is composed of small droplets of oil dispersed in water, while the W/O emulsion is composed of small droplets of water dispersed in oil. Different mixing processes may generate either O/W or W/O emulsions, to some extent independently of the water-to-lipid ratio. For the O/W emulsion, oil was added to the water in one step and mixed, while water was gradually added to the oil and mixed for the W/O emulsion. The visual appearance of these two 40:60 emulsions differs significantly. The O/W emulsion was white in liquid form, while the W/O emulsion was cream colored with a viscous texture. Measurements with the six-wavelength TD-DOS system were performed for the two types of 40:60 emulsions. The reduced scattering coefficient of the W/O emulsion at 908 nm was 10 cm⁻¹, which is in the range of human breast tissue, whereas the reduced scattering coefficient of the O/W emulsion at the same wavelength was 57 cm⁻¹. Figure 10 shows microscopic images of the two types of 40:60 emulsions. The size and number of particles were different for each emulsion; the O/W emulsion contained smaller particles with a higher density compared with the W/O emulsion. This characteristic was also qualitatively consistent with the obtained reduced scattering coefficients. After conducting a number of experiments, we decided to make phantoms with water-to-lipid ratios of 40:60, 20:80, and 5:95 with the W/O preparation procedure, which resulted in a better stability of the completed solid tissue phantoms. Although making all phantoms consistently with the W/O preparation procedure would have been desirable, the three emulsions with a higher percentage of water (99:1, 80:20 and 60:40) could not be solidified with the oil-solidifying agent when prepared according to this procedure. For this reason, the phantoms with water-to-lipid ratios of 99:1, 80:20, and 60:40 were made with the O/W preparation procedure. The so-prepared emulsion were less stable, but could be solidified.

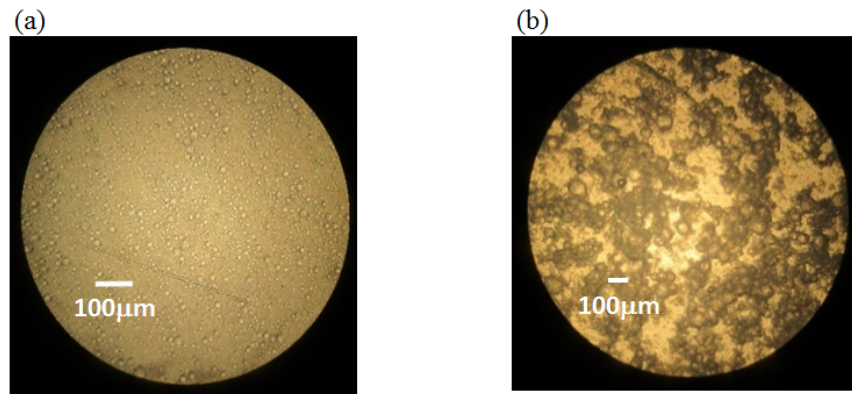


Fig. 10. 40:60 emulsions before solidification (a) O/W (200x magnification) and (b) W/O (100 x magnification).

4.2.2 Issues of liquid emulsion and solid phantom preparation for the 60:40 emulsion

As described in Section 2.3.2, the preparation procedure for the 60:40 emulsion had to be slightly modified compared to the simpler procedure used for 80:20 emulsion. When preparing the 60:40 emulsion in the same way as the 80:20 emulsion, the reduced scattering coefficient of the resulting phantom was much higher than that of human breast tissue, presumably due to a larger number of lipid emulsion particles in the 60:40 emulsion compared to the 80:20 emulsion. Another issue was that the 60:40 emulsion did not solidify.

After several experiments, we achieved scattering properties in the range of human breast tissue when we first added half of the final water mass as pure water until emulsified, then the remaining agar mixture in a second step. Following this procedure, we were also able to solidify the emulsion. This shows that the quality of a phantom depends both on applied procedures and compounding ratios of each ingredient. In this context, it should also be emphasized that it can be very helpful to determine the homogeneity of a phantom with MRI non-destructively since it cannot be verified from outside.

4.2.3 Issues of liquid emulsion and solid phantom preparation for the 99:1 emulsion

It would have been more convenient to prepare this phantom directly with undiluted Intralipos 20%. This emulsion is also very stable because it contains very small oil particles (diameter 97 nm) [37]. However, μ'_s of undiluted Intralipos 20% was found to be as large as 80 cm^{-1} at 908 nm, which renders this emulsion unsuitable for preparing phantoms mimicking human breast tissue with much smaller μ'_s values.

4.3 Evaluation of the solid tissue phantoms

The water and lipid volume fractions obtained with the TD-DOS system and MRI (see Fig. 8) correlated with the expected theoretical volume fractions based on the phantom preparation procedure. However, as the water content increased, the TD-DOS obtained water volume fractions were slightly lower than the expected values (see Fig. 8). The spectral features of water absorption depend on the water binding state and its temperature. It has been reported that the absorption of bound water decreases above and below 970 nm relative to free water in vivo [38], according to Fig.1 (b) in this reference. Since our phantoms were solidified with coagulants, it can be assumed that they were in the bound water state. However, the free water absorption spectrum was used as the extinction coefficient, $\epsilon_i(\lambda)$, for water to determine the water volume fractions at each wavelength according to Eq. (3). This difference might explain the underestimation of the water content. On the contrary, the water volume fractions obtained from TD-DOS measurements on the liquid emulsions before solidification

agreed well with the expected values based on the mixing procedure (data are not shown). Beside the effect of solidification, the absorption coefficient of solidifying agents might be higher than we expected even though we assumed that it is negligible. The optical parameters and the water and lipid contents of all solid phantoms were stable for a minimum of one month (see Fig. 9). Among these parameters, μ_a and water and lipid contents were stable for two months. The slight variations were confirmed in the optical parameters and the water and lipid contents. There is a possibility that the variations were caused by the temperature change inside the phantoms, though the phantoms were taken out from the refrigerator two hours prior to testing. The μ'_s of all phantoms were stable for one month, and the measurement error were less than 10% compared to the results measured on the first day. Since we measured the center of each phantom only once at each time point, the error could be improved by carrying out the measurement for several times. The changes in μ'_s were confirmed for all phantoms after one month, and their trend was different depending on the water-to-lipid ratio. The μ'_s of the phantoms with a low percentage of lipid (water-to-lipid ratio of 99:1, 80:20 and 60:40) increased slightly after one month. We suppose that this change was caused due to a little evaporation of water in the phantom. The μ'_s for the phantoms with a high percentage of lipid (water-to-lipid ratio of 40:60 and 20:80) decreased significantly after one month. This change is presumed to depend on the particle size of the emulsion, which changed through the agglomeration and coalescence of dissociated water and lipid particles. We could not confirm the change in μ'_s for the phantom with water-to-lipid ratio of 5:95. However, the dissociation of the water and lipid was occurred on the surface of the phantom.

There are some other issues that remain regarding the phantoms. The wavelength dependence of the reduced scattering coefficient as in the case of human tissues [39] was observed only for the phantom with water-to-lipid ratio of 99:1. We consider that it is caused by the difference of the particle size in each emulsion. The emulsion of 1% Intralipos was used for the phantom with water-to-lipid ratio of 99:1, and its particle size is 97 nm [37]. On the contrary, the particle size of the emulsion used for other water/lipid phantoms was larger than that of Intralipos. An example of the particle size of emulsion with water-to-lipid of 40:60 is shown in the Fig. 10(b). Since the wavelength dependence of the reduced scattering coefficient based on Mie theory becomes weak as the particle size increases, it was not observed or weak for water/lipid phantoms with water-to-lipid ratio of 80:20, 60:40, 40:60, 20:80, and 5:95 [40]. In this study, the amount of lecithin was fixed to 1 wt% of soybean oil. We found that the reduced scattering coefficients can be adjusted by changing the quantity of lecithin used and the emulsification temperature. In a future project we intend to study ways to improve the wavelength dependence of the reduced scattering coefficients of the phantoms, and processes to create them with the desired reduced scattering coefficients. Once this method is established, there is potential to adjust the absorption coefficients by adding ink and construct a phantom also mimicking tumors or cysts.

5. Conclusion

In this study, solid phantoms with controllable water-to-lipid ratios with long-term stability and reduced scattering coefficients in the range of human breast tissue were successfully made. For this purpose, different optimized protocols were devised for the preparation of emulsions with different water-to-lipid ratios and for their subsequent solidification. As a preparatory step, liquid emulsions with water-to-lipid ratio of 40:60 were made from distilled water and a combination of soybean oil and soybean lecithin. Water-in-oil (W/O) and oil-in-water (O/W) preparation procedures were compared in this case and resulted in different reduced scattering coefficients. The obtained liquid emulsion was stable only for a few hours, after which it gradually demulsified, accompanied by a change in optical properties. To overcome this issue, solidifying coagulants were added to retain the emulsion stability over a

prolonged period of time. We created a set of six solid phantoms consisting primarily of water and lipid, then evaluated them with our six-wavelength TD-DOS system and MRI. The obtained water-to-lipid volume fractions were close to the expected ones, which demonstrated the suitability of the phantom. Moreover, it was confirmed that the optical parameters and the water and lipid contents of the phantoms were stable for a minimum of one month. The results demonstrated that the proposed solid phantom series can be a useful tool to evaluate the performance and reproducibility of the NIRS system for measuring water and lipid contents. We are planning to conduct a further study of our TD-DOS system with these stable water/lipid phantoms to assess the system performance for monitoring chemotherapy effects on breast cancer patients.

Funding

Japan Society for the Promotion of Science (JSPS) KAKENHI Grant Numbers (JP15K19781 and JP17H03591).

Acknowledgments

We would like to thank Dr. Toshiaki Saeki and Dr. Shigeto Ueda, Department of Breast Oncology, International Medical Center, Saitama Medical University for useful discussions. This work was partially supported by JSPS KAKENHI.

Disclosures

The authors declare that they have no conflicts of interest.

References

1. F. Bevilacqua, A. J. Berger, A. E. Cerussi, D. Jakubowski, and B. J. Tromberg, "Broadband absorption spectroscopy in turbid media by combined frequency-domain and steady-state methods," *Appl. Opt.* **39**(34), 6498–6507 (2000).
2. D. Grosenick, K. T. Moesta, H. Wabnitz, J. Mücke, C. Stroszczynski, R. Macdonald, P. M. Schlag, and H. Rinneberg, "Time-domain optical mammography: initial clinical results on detection and characterization of breast tumors," *Appl. Opt.* **42**(16), 3170–3186 (2003).
3. Q. Fang, S. A. Carp, J. Selb, G. Boverman, Q. Zhang, D. B. Kopans, R. H. Moore, E. L. Miller, D. H. Brooks, and D. A. Boas, "Combined optical imaging and mammography of the healthy breast: optical contrast derived from breast structure and compression," *IEEE Trans. Med. Imaging* **28**(1), 30–42 (2009).
4. Y. Ueda, K. Yoshimoto, E. Ohmae, T. Suzuki, T. Yamanaka, D. Yamashita, H. Ogura, C. Teruya, H. Nasu, E. Ima, H. Sakahara, M. Oda, and Y. Yamashita, "Time-resolved optical mammography and its preliminary clinical results," *Technol. Cancer Res. Treat.* **10**(5), 393–401 (2011).
5. P. G. Anderson, J. M. Kainerstorfer, A. Sassaroli, N. Krishnamurthy, M. J. Homer, R. A. Graham, and S. Fantini, "Broadband optical mammography: chromophore concentration and hemoglobin saturation contrast in breast cancer," *PLoS One* **10**(3), e0117322 (2015).
6. P. Taroni, A. M. Paganoni, F. Ieva, A. Pifferi, G. Quarto, F. Abbate, E. Cassano, and R. Cubeddu, "Non-invasive optical estimate of tissue composition to differentiate malignant from benign breast lesions: A pilot study," *Sci. Rep.* **7**(1), 40683 (2017).
7. N. Yoshizawa, Y. Ueda, H. Nasu, H. Ogura, E. Ohmae, K. Yoshimoto, Y. Takehara, Y. Yamashita, and H. Sakahara, "Effect of the chest wall on the measurement of hemoglobin concentrations by near-infrared time-resolved spectroscopy in normal breast and cancer," *Breast Cancer* **23**(6), 844–850 (2016).
8. Y. Zhao, B. W. Pogue, S. J. Haider, J. Gui, R. M. diFlorio-Alexander, K. D. Paulsen, and S. Jiang, "Portable, parallel 9-wavelength near-infrared spectral tomography (NIRST) system for efficient characterization of breast cancer within the clinical oncology infusion suite," *Biomed. Opt. Express* **7**(6), 2186–2201 (2016).
9. B. J. Tromberg, A. Cerussi, N. Shah, M. Compton, A. Durkin, D. Hsiang, J. Butler, and R. Mehta, "Imaging in breast cancer: diffuse optics in breast cancer: detecting tumors in pre-menopausal women and monitoring neoadjuvant chemotherapy," *Breast Cancer Res.* **7**(6), 279–285 (2005).
10. T. D. O'Sullivan, A. Leproux, J. H. Chen, S. Bahri, A. Matlock, D. Roblyer, C. E. McLaren, W. P. Chen, A. E. Cerussi, M. Y. Su, and B. J. Tromberg, "Optical imaging correlates with magnetic resonance imaging breast density and reveals composition changes during neoadjuvant chemotherapy," *Breast Cancer Res.* **15**(1), R14 (2013).
11. S. Jiang, B. W. Pogue, P. A. Kaufman, J. Gui, M. Jermyn, T. E. Frazee, S. P. Poplack, R. DiFlorio-Alexander, W. A. Wells, and K. D. Paulsen, "Predicting breast tumor response to neoadjuvant chemotherapy with diffuse optical spectroscopic tomography prior to treatment," *Clin. Cancer Res.* **20**(23), 6006–6015 (2014).

12. S. Ueda, I. Kuji, T. Shigekawa, H. Takeuchi, H. Sano, E. Hirokawa, H. Shimada, H. Suzuki, M. Oda, A. Osaki, and T. Saeki, "Optical imaging for monitoring tumor oxygenation response after initiation of single-agent bevacizumab followed by cytotoxic chemotherapy in breast cancer patients," *PLoS One* **9**(6), e98715 (2014).
13. B. J. Tromberg, Z. Zhang, A. Leproux, T. D. O'Sullivan, A. E. Cerussi, P. M. Carpenter, R. S. Mehta, D. Roblyer, W. Yang, K. D. Paulsen, B. W. Pogue, S. Jiang, P. A. Kaufman, A. G. Yodh, S. H. Chung, M. Schnall, B. S. Snyder, N. Hylton, D. A. Boas, S. A. Carp, S. J. Isakoff, and D. Mankoff, "Predicting responses to neoadjuvant chemotherapy in breast cancer: ACRIN 6691 trial of diffuse optical spectroscopic imaging," *Cancer Res.* **76**(20), 5933–5944 (2016).
14. L. Spinelli, F. Martelli, A. Farina, A. Pifferi, A. Torricelli, R. Cubeddu, and G. Zaccanti, "Calibration of scattering and absorption properties of a liquid diffusive medium at NIR wavelengths. Time-resolved method," *Opt. Express* **15**(11), 6589–6604 (2007).
15. L. Spinelli, M. Botwicz, N. Zolek, M. Kacprzak, D. Milej, P. Sawosz, A. Liebert, U. Weigel, T. Durduran, F. Foschum, A. Kienle, F. Baribeau, S. Leclair, J.-P. Bouchard, I. Noiseux, P. Gallant, O. Mermut, A. Farina, A. Pifferi, A. Torricelli, R. Cubeddu, H.-C. Ho, M. Mazurenka, H. Wabnitz, K. Klauenberg, O. Bodnar, C. Elster, M. Bénazech-Lavoué, Y. Bérubé-Lauzière, F. Lesage, D. Khoptyar, A. A. Subash, S. Andersson-Engels, P. Di Ninni, F. Martelli, and G. Zaccanti, "Determination of reference values for optical properties of liquid phantoms based on Intralipid and India ink," *Biomed. Opt. Express* **5**(7), 2037–2053 (2014).
16. B. W. Pogue and M. S. Patterson, "Review of tissue simulating phantoms for optical spectroscopy, imaging and dosimetry," *J. Biomed. Opt.* **11**(4), 041102 (2006).
17. S. Merritt, G. Gulsen, G. Chiou, Y. Chu, C. Deng, A. E. Cerussi, A. J. Durkin, B. J. Tromberg, and O. Nalcioğlu, "Comparison of water and lipid content measurements using diffuse optical spectroscopy and MRI in emulsion phantoms," *Technol. Cancer Res. Treat.* **2**(6), 563–569 (2003).
18. G. Quarto, A. Pifferi, I. Bargigia, A. Farina, R. Cubeddu, and P. Taroni, "Recipes to make organic phantoms for diffusive optical spectroscopy," *Appl. Opt.* **52**(11), 2494–2502 (2013).
19. R. Nachabé, B. H. Hendriks, A. E. Desjardins, M. van der Voort, M. B. van der Mark, and H. J. Sterenborg, "Estimation of lipid and water concentrations in scattering media with diffuse optical spectroscopy from 900 to 1,600 nm," *J. Biomed. Opt.* **15**(3), 037015 (2010).
20. K. E. Michaelsen, V. Krishnaswamy, A. Shenoy, E. Jordan, B. W. Pogue, and K. D. Paulsen, "Anthropomorphic breast phantoms with physiological water, lipid, and hemoglobin content for near-infrared spectral tomography," *J. Biomed. Opt.* **19**(2), 026012 (2014).
21. N. Yoshizawa, Y. Ueda, T. Mimura, E. Ohmae, K. Yoshimoto, H. Wada, H. Ogura, and H. Sakahara, "Factors affecting measurement of optic parameters by time-resolved near-infrared spectroscopy in breast cancer," *J. Biomed. Opt.* **23**(2), 026010 (2018).
22. K. Yamazaki, K. Suzuki, H. Itoh, K. Muramatsu, K. Nagahashi, N. Tamura, T. Uchida, K. Sugihara, H. Maeda, and N. Kanayama, "Cerebral oxygen saturation evaluated by near-infrared time-resolved spectroscopy (TRS) in pregnant women during caesarean section - a promising new method of maternal monitoring," *Clin. Physiol. Funct. Imaging* **33**(2), 109–116 (2013).
23. K. Yoshitani, K. Kuwajima, T. Irie, Y. Inatomi, A. Miyazaki, K. Iihara, and Y. Ohnishi, "Clinical validity of cerebral oxygen saturation measured by time-resolved spectroscopy during carotid endarterectomy," *J. Neurosurg. Anesthesiol.* **25**(3), 248–253 (2013).
24. S. Koga, T. J. Barstow, D. Okushima, H. B. Rossiter, N. Kondo, E. Ohmae, and D. C. Poole, "Validation of a high-power, time-resolved, near-infrared spectroscopy system for measurement of superficial and deep muscle deoxygenation during exercise," *J. Appl. Physiol.* **118**(11), 1435–1442 (2015).
25. S. Nirengi, T. Yoneshiro, H. Sugie, M. Saito, and T. Hamaoka, "Human brown adipose tissue assessed by simple, noninvasive near-infrared time-resolved spectroscopy," *Obesity* **23**(5), 973–980 (2015).
26. A. Liebert, H. Wabnitz, D. Grosenick, M. Möller, R. Macdonald, and H. Rinneberg, "Evaluation of optical properties of highly scattering media by moments of distributions of times of flight of photons," *Appl. Opt.* **42**(28), 5785–5792 (2003).
27. M. S. Patterson, B. Chance, and B. C. Wilson, "Time resolved reflectance and transmittance for the non-invasive measurement of tissue optical properties," *Appl. Opt.* **28**(12), 2331–2336 (1989).
28. A. H. Hielscher, S. L. Jacques, L. Wang, and F. K. Tittel, "The influence of boundary conditions on the accuracy of diffusion theory in time-resolved reflectance spectroscopy of biological tissues," *Phys. Med. Biol.* **40**(11), 1957–1975 (1995).
29. K. Suzuki, Y. Yamashita, K. Ohta, M. Kaneko, M. Yoshida, and B. Chance, "Quantitative measurement of optical parameters in normal breasts using time-resolved spectroscopy: in vivo results of 30 Japanese women," *J. Biomed. Opt.* **1**(3), 330–334 (1996).
30. A. Liebert, H. Wabnitz, D. Grosenick, and R. Macdonald, "Fiber dispersion in time domain measurements compromising the accuracy of determination of optical properties of strongly scattering media," *J. Biomed. Opt.* **8**(3), 512–516 (2003).
31. R. L. P. van Veen, H. J. Sterenborg, A. Pifferi, A. Torricelli, E. Chikoidze, and R. Cubeddu, "Determination of visible near-IR absorption coefficients of mammalian fat using time- and spatially resolved diffuse reflectance and transmission spectroscopy," *J. Biomed. Opt.* **10**(5), 054004 (2005).
32. A. E. Cerussi, V. W. Tanamai, R. S. Mehta, D. Hsiang, J. Butler, and B. J. Tromberg, "Frequent optical imaging during breast cancer neoadjuvant chemotherapy reveals dynamic tumor physiology in an individual patient," *Acad. Radiol.* **17**(8), 1031–1039 (2010).

33. S. J. Matcher, M. Cope, and D. T. Delpy, "Use of the water absorption spectrum to quantify tissue chromophore concentration changes in near-infrared spectroscopy," *Phys. Med. Biol.* **39**(1), 177–196 (1994).
34. S. D. Serai, J. R. Dillman, and A. T. Trout, "Proton density fat fraction measurements at 1.5- and 3-T hepatic MR imaging: same-day agreement among readers and across two imager manufacturers," *Radiology* **284**(1), 244–254 (2017).
35. D. Hernando, S. D. Sharma, M. Aliyari Ghasabeh, B. D. Alvis, S. S. Arora, G. Hamilton, L. Pan, J. M. Shaffer, K. Sofue, N. M. Szevenyi, E. B. Welch, Q. Yuan, M. R. Bashir, I. R. Kamel, M. J. Rice, C. B. Sirlin, T. Yokoo, and S. B. Reeder, "Multisite, multivendor validation of the accuracy and reproducibility of proton-density fat-fraction quantification at 1.5T and 3T using a fat-water phantom," *Magn. Reson. Med.* **77**(4), 1516–1524 (2017).
36. J. Schindelin, I. Arganda-Carreras, E. Frise, V. Kaynig, M. Longair, T. Pietzsch, S. Preibisch, C. Rueden, S. Saalfeld, B. Schmid, J. Y. Tinevez, D. J. White, V. Hartenstein, K. Eliceiri, P. Tomancak, and A. Cardona, "Fiji: an open-source platform for biological-image analysis," *Nat. Methods* **9**(7), 676–682 (2012).
37. H. J. van Staveren, C. J. Moes, J. van Marie, S. A. Prahl, and M. J. van Gemert, "Light scattering in Intralipid-10% in the wavelength range of 400–1100 nm," *Appl. Opt.* **30**(31), 4507–4514 (1991).
38. S. H. Chung, H. Yu, M. Y. Su, A. E. Cerussi, and B. J. Tromberg, "Molecular imaging of water binding state and diffusion in breast cancer using diffuse optical spectroscopy and diffusion weighted MRI," *J. Biomed. Opt.* **17**(7), 071304 (2012).
39. S. L. Jacques, "Optical properties of biological tissues: a review," *Phys. Med. Biol.* **58**(11), R37–R61 (2013).
40. R. Graaff, J. G. Aarnoudse, J. R. Zijp, P. M. A. Sloot, F. F. M. de Mul, J. Greve, and M. H. Koelink, "Reduced light-scattering properties for mixtures of spherical particles: a simple approximation derived from Mie calculations," *Appl. Opt.* **31**(10), 1370–1376 (1992).